Paleoceanography and Paleoclimatology

RESEARCH ARTICLE
10.1029/2018PA003366

# Isolating and Reconstructing Key Components of North Atlantic Ocean Variability From a Sclerochronological Spatial Network

D. J. Reynolds[1], I. R. Hall[1], S. M. Slater[1], M. J. Mette[2], A. D. Wanamaker[2], J. D. Scourse[3], F. K. Garry[4], and P. R. Halloran[4]

[1]School of Earth and Ocean Sciences, Cardiff University, Cardiff, UK, [2]Department of Geological and Atmospheric Sciences, Iowa State University, Ames, Iowa, USA, [3]College of Life and Environmental Sciences, University of Exeter, Penryn, UK, [4]College of Life and Environmental Sciences, Exeter University, Exeter, UK

**Abstract** Our understanding of North Atlantic Ocean variability within the coupled climate system is limited by the brevity of instrumental records and a deficiency of absolutely dated marine proxies. Here we demonstrate that a spatial network of marine stable oxygen isotope series derived from molluscan sclerochronologies ($\delta^{18}O_{shell}$) can provide skillful annually resolved reconstructions of key components of North Atlantic Ocean variability with absolute dating precision. Analyses of the common $\delta^{18}O_{shell}$ variability, using principal component analysis, highlight strong connections with tropical North Atlantic and subpolar gyre (SPG) sea surface temperatures and sea surface salinity in the North Atlantic Current (NAC) region. These analyses suggest that low-frequency variability is dominated by the tropical Atlantic signal while decadal variability is dominated by variability in the SPG and salinity transport in the NAC. Split calibration and verification statistics indicate that the composite series produced using the principal component analysis can provide skillful quantitative reconstructions of tropical North Atlantic and SPG sea surface temperatures and NAC sea surface salinities over the industrial period (1864–2000). The application of these techniques with extended individual $\delta^{18}O_{shell}$ series provides powerful baseline records of past North Atlantic variability into the unobserved preindustrial period. Such records are essential for developing our understanding of natural climate variability in the North Atlantic Ocean and the role it plays in the wider climate system, especially on multidecadal to centennial time scales, potentially enabling reduction of uncertainties in future climate predictions.

**Key Points:**
- Despite originating from coastal shelf sea environments across the North Atlantic Ocean, molluscan $\delta^{18}O$ series exhibit significant coherence
- A network of multiple molluscan $\delta^{18}O$ records provides skillful quantitative reconstructions of key components of North Atlantic variability
- These reconstructions provide novel information about tropical North Atlantic and SPG SSTs and salinity in the North Atlantic Current

**Supporting Information:**
- Supporting Information S1

**Correspondence to:**
D. J. Reynolds,
davidreynolds@email.arizona.edu

**Citation:**
Reynolds, D. J., Hall, I. R., Slater, S. M., Mette, M. J., Wanamaker, A. D., Scourse, J. D., et al. (2018). Isolating and reconstructing key components of North Atlantic Ocean variability from a sclerochronological spatial network. *Paleoceanography and Paleoclimatology*, *33*, 1086–1098. https://doi.org/10.1029/2018PA003366

Received 15 MAR 2018
Accepted 26 SEP 2018
Accepted article online 29 SEP 2018
Published online 22 OCT 2018



## 1. Main Text

Our understanding of past North Atlantic circulation dynamics and the influence these changes have on the wider climate system are limited both by the short temporal and limited spatial distribution of marine observations, as well as by the large uncertainties typical of proxy reconstructions dated using radiocarbon-derived age models (typically ±100 years). While sediment core records provide invaluable baseline records of past marine variability, their associated age model uncertainties preclude the analysis of multiple cores to resolve decadal or subdecadal scale changes in the spatial patterns of marine variability. Spatial networking techniques have facilitated the reconstruction of regional to hemispheric-scale modes (i.e., patterns) of atmospheric variability based on the analysis of suites of absolutely dated, via band counting and crossdating, tree ring series (dendrochronologies; e.g., Moberg et al., 2005; Wilson et al., 2016). The precisely dated nature of the dendrochronologies, based on crossdating (Black et al., 2016), enables the assessment of the absolute timing of variability between these climate records constructed across broad geographical regions; local changes affecting single proxy records are "averaged out," allowing the common variability across the network to be identified (Wilson et al., 2010). While such techniques have been extensively used in terrestrial paleoclimatology, the lack of absolutely dated and annually resolved marine climate records has precluded this approach being widely used in the marine environment. Currently, in the extratropical North Atlantic, investigations of marine proxy networks have been *limited to the evaluation of low frequency* (*centennial*) *ocean variability* (e.g., Cunningham et al., 2013; McGregor et al., 2015), with high frequency (decadal/subdecadal) marine variability being derived through extrapolation of terrestrial proxy networks, largely dendrochronologies, on adjacent landmasses (e.g., Gray, 2004; Mann et al., 2009; Rahmstorf et al., 2015). It is important to note that the application of these terrestrial tree ring proxy

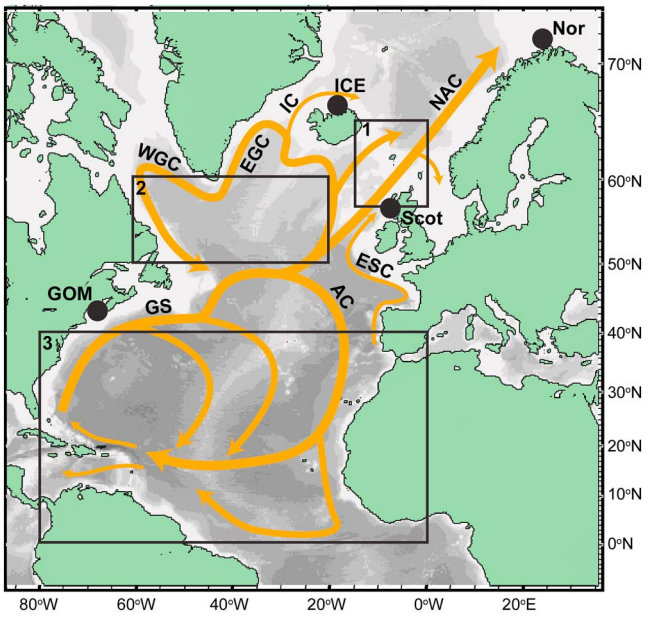


**Figure 1.** A schematic of the North Atlantic Ocean surface currents (orange arrows) and the sampling localities (black circles) of stable oxygen isotope series used to construct the $\delta^{18}O_{PC1\text{-}S1\text{-}S3}$ composite. Ice = Iceland; Nor = Norway; Scot = Scotland; GOM = Gulf of Maine; NAC = North Atlantic Current; GS = Gulf Stream; EGC = East Greenland Current; WGC = West Greenland Current; ESC = European Slope Current; IC = Irminger Current; AC = Azores Current. The black boxes 1–3 denote the regions from which sea surface temperature and sea surface salinity (SSS) were obtained from the HadISST1 and EN4 SSS gridded data sets for the environmental analyses. Box 1 represents North Atlantic Current waters, box 2 broadly represents the North Atlantic subpolar gyre, and box 3 represents the tropical North Atlantic. Bathymetry data provided by Global Bathymetric Chart of the Oceans (GEBCO; https://www.gebco.net) plotted in GeoMapApp (www.geomapapp.org). Ocean circulation modified from Marzocchi et al. (2015).

networks to derive an ocean climate field reconstruction prevents the independent examination of the influence that marine variability has on, for example, Northern Hemispheric surface air temperatures, as the reconstructions of Northern Hemispheric surface air temperatures incorporate the same tree ring records.

Here we demonstrate the potential for utilizing a spatial network of precisely dated marine molluscan stable oxygen isotope ($\delta^{18}O_{shell}$) series to reconstruct interannual to multidecadal variability in the North Atlantic Ocean over the industrial era. Molluscan sclerochronologies, a marine counterpart to dendrochronologies, provide a basis for the direct application of spatial networking techniques given their absolutely dated and annually resolved nature. In recent years, absolutely dated $\delta^{18}O_{shell}$ records have been developed from sites located in Scotland (Reynolds, Hall, et al., 2017), Norway (Mette et al., 2016), Iceland (Reynolds et al., 2016), and the Gulf of Maine (Wanamaker et al., 2008). These records, based on the $\delta^{18}O$ analysis of carbonate samples derived from the cross-dated annual growth increments of the long-lived bivalve molluscs *Arctica islandica* and *Glycymeris glycymeris*, each demonstrates significant sensitivity to broad scale North Atlantic Ocean variability. While these four independent records represent a seemingly small marine proxy network relative to the abundance of records included in dendrochronological-derived spatial networks, observation-based analysis at the four sampling locations supports their value in reconstructing broad scale North Atlantic variability.

This study therefore sets out to (1) investigate the potential of generating statistically significant composite series using principal component analysis (PCA) on multiple $\delta^{18}O_{shell}$ series from the continental shelf seas of the North Atlantic, (2) investigate the sensitivity of the resulting composite series to broad scale variability in sea surface temperatures (SSTs) and sea surface salinities (SSSs) in the North Atlantic Ocean, and (3) quantitatively evaluate the skill of the composite series at reconstructing components of North Atlantic variability. Our proof of concept approach used here will enable future workers to apply similar statistical techniques as more sclerochronological records become available.

## 2. Methodology

### 2.1. Sampling Locations and Individual $\delta^{18}O_{shell}$ Series

In this study we utilize four independently constructed $\delta^{18}O_{shell}$ series derived from the annually-resolved shell growth increments of the long-lived marine bivalve molluscs *A. islandica* and *G. glycymeris* (Table S1 in the supporting information). The four independent $\delta^{18}O_{shell}$ series were constructed by analyzing the oxygen isotope composition of annual growth increments from shell material that was collected from the shelf seas off the coasts of Scotland, Gulf of Maine (USA), North Iceland, and North Norway (Figure 1 and Table S1). The shells were collected from 6- to 80-m water depth. The individual $\delta^{18}O_{shell}$ series span a range of time intervals with the shortest spanning the 20th century (Norway; Mette et al., 2016) and the longest spanning the entirety of the last millennium (North Iceland; Reynolds et al., 2016). Preliminary analyses of the covariance between the four records were conducted using linear regression analyses over the record's coeval period of 1900–2000. The significance of the regressions was tested using the Ebisuzaki Monte Carlo methodology to take account for autocorrelation contained in each of the time series (Ebisuzaki, 1997). The $\delta^{18}O_{shell}$ data from each series are shown in Figure S1 in the supporting information.

### 2.2. Spatial Network Construction and Validation

To extract the common variability recorded across the four individual $\delta^{18}O_{shell}$ series we used a nested PCA approach (Cunningham et al., 2013; Wilson et al., 2010). To evaluate the possible influence of variable

(nonstationary) coherence between the four locations that may occur in response to, for example, changes in atmospheric and/or ocean circulation patterns over the wider North Atlantic region, the PCA analyses were conducted using three differing strategies. Strategy 1 was a conventional nested PCA using the longest period of overlap between the four series (1900–2000) with the resulting principal component (PC) providing the primary nest. The shortest independent $\delta^{18}O_{shell}$ series (Norway) was then removed and the PCA repeated using the remaining three independent $\delta^{18}O_{shell}$ series for their coeval period. The resulting PC provided the secondary nest (1864–2000). The interval of the secondary nest not represented in the primary nest (1864–1899) was then combined, with no overlap, to provide a final strategy 1 composite series (1864–2000). In strategy 2, the four independent $\delta^{18}O_{shell}$ series were split into three nonoverlapping bins with periods spanning 1901–1950, 1951–2000 (containing all four series), and 1864–1900 (containing the three longest series, i.e., Norway removed), respectively. PCA was then conducted on the three bins independently, generating PCs for each time period. The PCs from each bin were then combined with no period of overlap to create a final strategy 2 composite series that spans 1864–2000. In the last approach, Strategy 3, the four independent $\delta^{18}O_{shell}$ series were split into 30 year bins, with each bin overlapping by 20 years. The PCA was then conducted on each 30 year bin and the PCs combined by arithmetically averaging the overlapping years to create a final strategy 3 composite series that spans 1864–2000. Strategies 2 and 3 were adopted as they provided at least three bins across the 1864–2000 period with sufficient data to conduct the PCA (i.e., at least three independent $\delta^{18}O_{shell}$ series and $\geq$30-year duration). In each strategy a minimum of three independent $\delta^{18}O_{shell}$ series contributed to the resulting composite series throughout the 1864–2000 period. Eigenvalue and percentage variance statistics were used to evaluate the significance of the PCs produced across all nests using each PCA strategy. Nests that contained eigenvalues $<1$ were omitted from the final composite series. The primary PCs extracted from the three PCA strategies are referred to hereafter as $\delta^{18}O_{PC1\text{-}S1}$, $\delta^{18}O_{PC1\text{-}S2}$, and $\delta^{18}O_{PC1\text{-}S3}$, respectively, and collectively referred to as $\delta^{18}O_{PC1\text{-}S1\text{-}3}$. The second PCs produced are referred to as $\delta^{18}O_{PC2\text{-}S1}$ and $\delta^{18}O_{PC2\text{-}S2}$, respectively. Due to a lack of significance (eigenvalues $< 1$) no tertiary PCs were extracted using strategies 1 and 2 and no secondary or tertiary PCs were extracted using strategy 3. PCAs were conducted using SBSS statistics v20 and PAST V3.18. Figure 2 shows the summary data for each of the PCA strategies whilst. Figure S2 shows a schematic diagram representing the construction of each of the three strategies, the time interval represented by each of the nests and the respective $\delta^{18}O_{shell}$ series each nest contains.

It is important to note that recalculating the PCA across multiple bins and then combining the resulting PCs (as in strategies 2 and 3) acts to remove the low frequency variability (effectively acting as a high pass filter) due to the data normalization required in the calculation of the PCA in each bin. As a result, the $\delta^{18}O_{PC1\text{-}S2}$ and $\delta^{18}O_{PC1\text{-}S3}$ series only contain variability on time scales $<$50 and $<$30 years, respectively. Therefore, to assess the influence our binning strategy might have had on the resulting composite series, the PCA was repeated, using strategy 1, but based on independent $\delta^{18}O_{shell}$ data initially treated using a range of first-order loess high pass filter ranging between 10 and 200 years, respectively. The resulting composite records generated, which each span the 1900–2000 interval and contain all four individual $\delta^{18}O_{shell}$ records, are referred to as $\delta^{18}O_{PC1\text{-}F}$.

### 2.3. Evaluating the Influence of the Number of Proxy Series in the Spatial Network

Given the relatively low number of independent $\delta^{18}O_{shell}$ series utilized it is important to assess the sensitivity of the composite $\delta^{18}O_{PC1\text{-}S1\text{-}3}$ series to potential biases associated with an individual $\delta^{18}O_{shell}$ series. To do this, the strategy 1 PCA was repeated with the omission of one individual $\delta^{18}O_{shell}$ series (Table S3). The PCA was replicated an additional 4 times, each time omitting a different independent $\delta^{18}O_{shell}$ series, but always containing at least three $\delta^{18}O_{shell}$ series. In total this approach generated five primary PCs, one containing all four independent $\delta^{18}O_{shell}$ series and four composites containing three independent $\delta^{18}O_{shell}$ series, each spanning the interval from 1900 to 2000. The PCA statistics and linear regression analyses, evaluated using the Ebisuzaki Monte Carlo methodology, conducted between each of the primary PCs, were then used to evaluate the relative influence of the independent $\delta^{18}O_{shell}$ series on the $\delta^{18}O_{PC1\text{-}S1}$ series (Figure S3 and Table S3).

The $\delta^{18}O_{PC1\text{-}S1\text{-}3}$ series were compared with pseudo primary PCs derived using PCA on the gridded SST, SSS data products, and the predicted $\delta^{18}O$ composition of aragonite ($\delta^{18}O_{syn}$) at each of the four locations for the period 1900–2000. The PCA was conducted using SST (HadISST1; Rayner et al., 2003) and SSS (EN4 SSS; Good

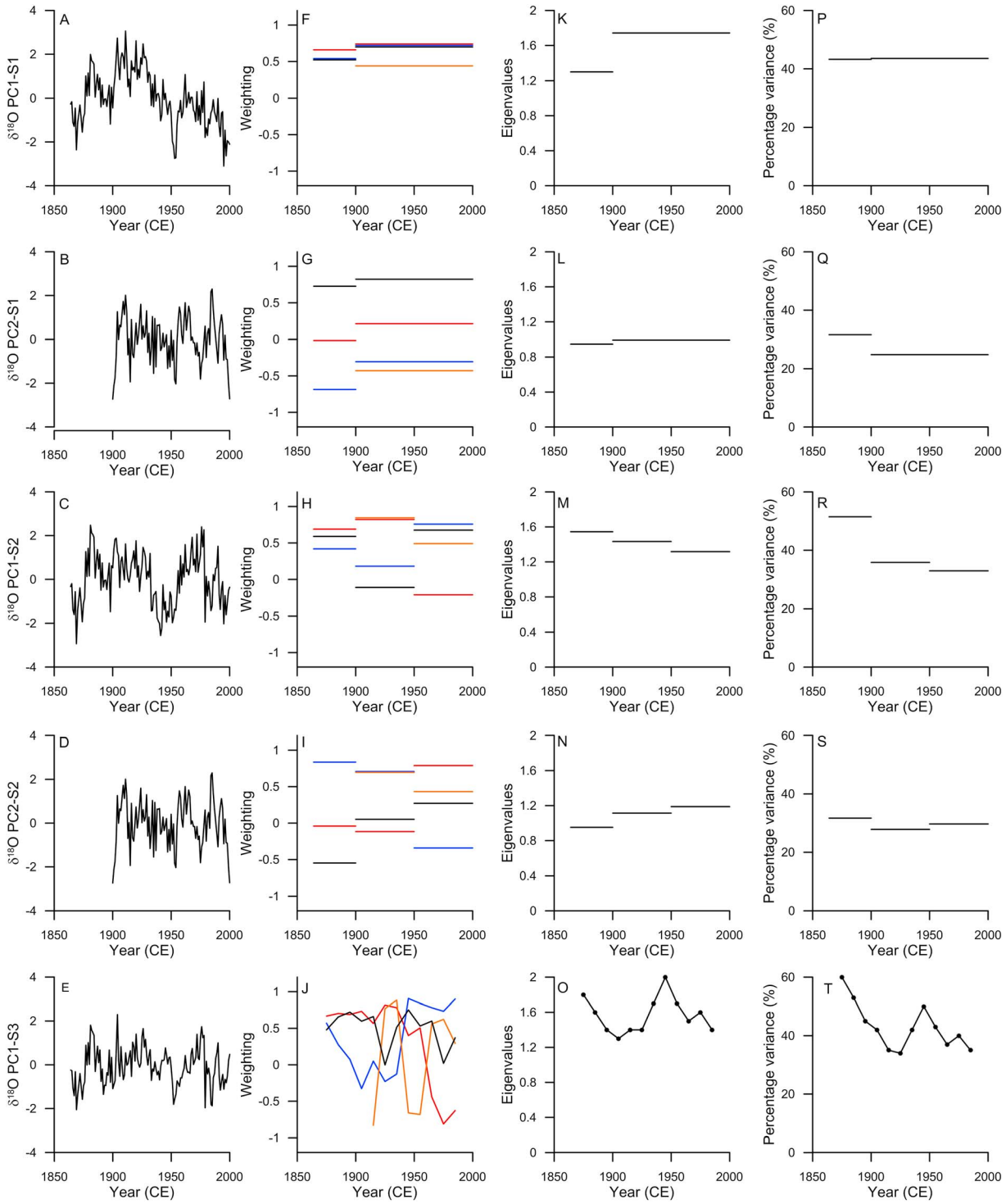


**Figure 2.** Comparison between principal components (PCs) generated using the three strategies for conducting the principal component analysis (PCA) and relative weighting of the isotope series on the PC. (a–e) The nested principal component outputs of the PCA using strategies 1 to 3, respectively. (f–j) The relative weighting of the four independent $\delta^{18}O_{shell}$ series in each of the PCs. The red line represents the Scottish $\delta^{18}O_{shell}$ series, the orange represents the Norwegian $\delta^{18}O_{shell}$ series, the black line represents the Gulf of Maine $\delta^{18}O_{shell}$ series, and the blue line the $\delta^{18}O_{shell}$ series from North Iceland. (k–o) Eigenvalue and (p–t) percentage variance statistics for each of the $\delta^{18}O_{PC1\text{-}S1\text{–}3}$ and $\delta^{18}O_{PC2\text{-}S1\text{–}2}$.

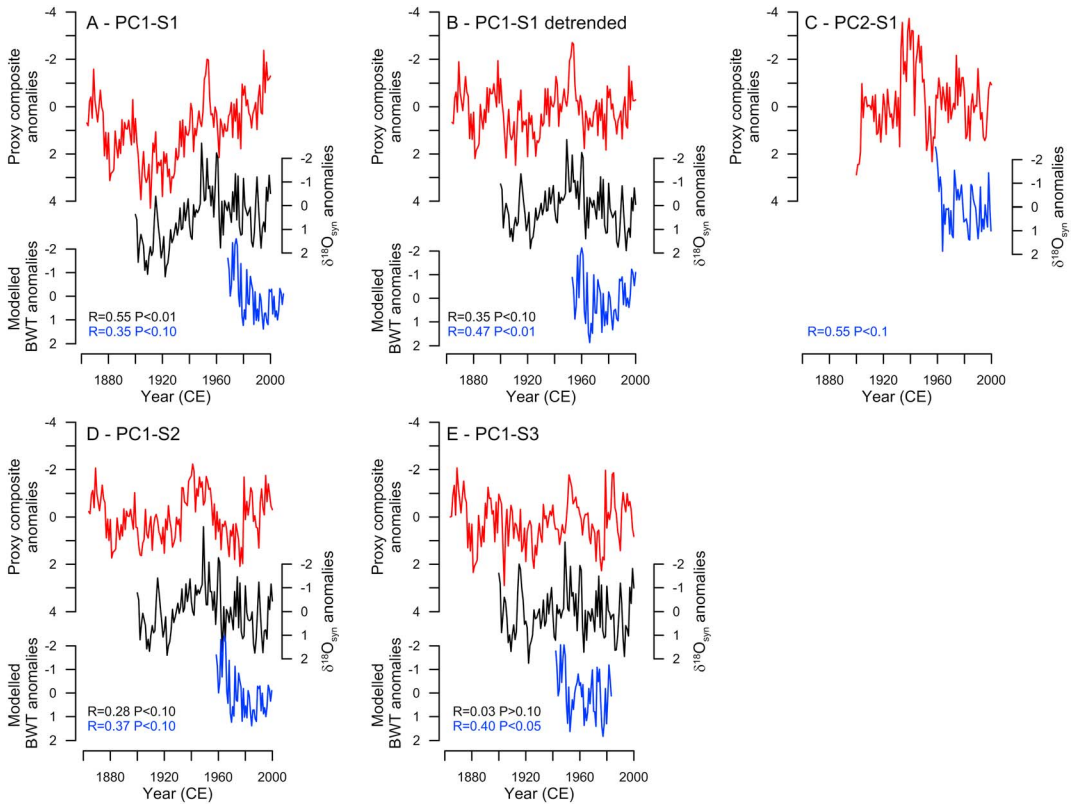


**Figure 3.** Comparison between the $\delta^{18}O_{PC\text{-}S1\text{–}3}$ series (red lines), $\boldsymbol{\delta}^{18}O_{syn\text{-}PC1\text{-}S1\text{–}3}$ (black lines), and model (blue lines) derived composite series generated using the three principal component analysis strategies. The corresponding correlation coefficients and Monte Carlo derived probabilities calculated between the proxy composites against the pseudo proxy and model derived composites are provided in blue and black text, respectively. Correlations are calculated using the annually resolved data. No $\boldsymbol{\delta}^{18}O_{syn\text{-}PC2\text{-}S1}$ series is plotted in (c) as the eigenvalues for this series are not significant (<1). Peak correlations between the $\delta^{18}O_{PC\text{-}S1\text{–}3}$ series and $\delta^{18}O_{syn\text{-}S1\text{-}S3}$ were obtained with zero year lag. However, peak correlations between the $\delta^{18}O_{PC1S\text{-}3}$ series and modeled data were obtained with the modeled data lagging the proxy composite by 4 to 6 years.

et al., 2013) data derived from 2 × 2° grid boxes from each of the four sampling locations and the primary PCs extracted (referred to hereafter as $SST_{PC1}$ and $SSS_{PC1}$; Figures 3 and S6). While there are uncertainties associated with gridded data products, associated with the reduced number of observations during the early half of the 20th century (Figure S4), these pseudo data still provide a useful test of the skill of the composite series at capturing the long-term variability in the North Atlantic system. Replication of these analyses using different gridded data products (e.g., ER SST V3 [Smith et al., 2008], ICOADs [Freeman et al., 2017], and HadSST3 [Kennedy et al., 2011]) suggests that the results are consistent regardless of the data product used (Figure S5). The $\delta^{18}O_{syn}$ data were generated using the Grossman and Ku (1986) aragonite paleotemperature equation coupled with the local salinity mixing line equations at each of the four sites (Cage & Austin, 2010; Mette et al., 2016; Smith et al., 2005; Whitney et al., 2017) to convert from local SST and SSS data to $\delta^{18}O_{syn}$. PCA was then conducted, using all three strategies, on the four independent $\delta^{18}O_{syn}$ records to derive the $\delta^{18}O_{syn\text{-}PC1\text{-}S1\text{-}3}$ composite records. These instrumental composites ($SST_{PC1}$, $SSS_{PC1}$, and $\delta^{18}O_{syn\text{-}PC1\text{-}s1\text{-}3}$), spanning 1900–2000, were correlated against the coeval $\delta^{18}O_{PC1\text{-}S1\text{-}3}$ series, and the significance tested using the Ebisuzaki Monte Carlo methodology, to evaluate the relative influence of SST and SSS on the $\delta^{18}O_{PC1\text{-}S1}$ series.

As the bivalve molluscs lived (and recorded environmental conditions) at their collection water depths between 6- and 80-m water, an additional suite of composite series was generated to assess any potential differences in the comparison with observational sea surface parameters. As no instrumental measurements of bottom water temperature (or salinity) data are available at the four sampling locations, we conducted the PCA, using all three strategies, based on modeled bottom water temperatures at each site. The bottom water temperature data were obtained from an adaption of a 1-D physical-biogeochemical model S2P3-R (v1.0;

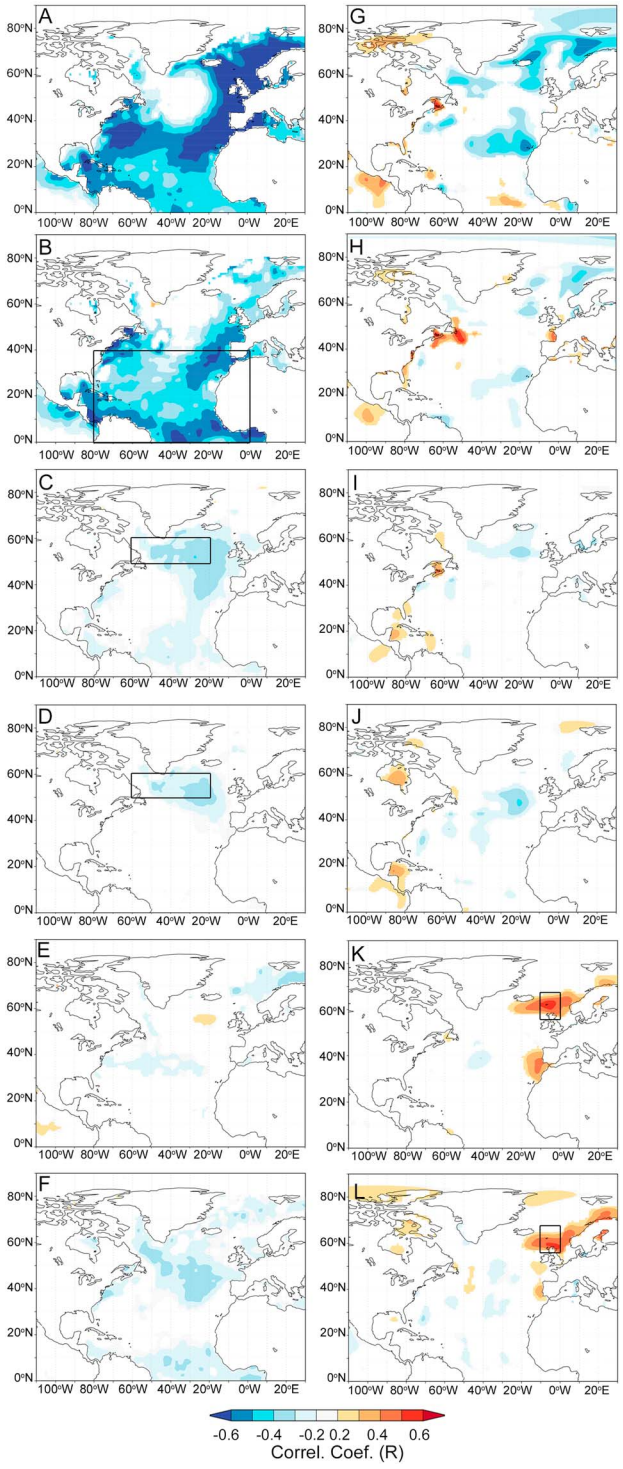


**Figure 4.** Point correlations calculated between the gridded sea surface temperatures (a–f, HadISST1) and sea surface salinities (g–l, EN4 SSS) correlated against (a and g) the $\delta^{18}O_{syn}$ series, (b and h) the $\delta^{18}O_{PC1\text{-}S1}$ series, (c and i) the 100-year first-order loess high pass filtered $\delta^{18}O_{PC1\text{-}S1}$ series, (d and j) the $\delta^{18}O_{PC1\text{-}S3}$ series, (e and k) the $\delta^{18}O_{PC2\text{-}S1}$ series, and (f and l) the $\delta^{18}O_{PC1\text{-}S2}$ series. Point correlations calculated using annual resolution data over the entire 20th century and are significant at $P < 0.1$ level. The correlations were conducted using KNMI Climate Explorer (https://climexp.knmi.nl/).

Marsh et al., 2015) driven by National Centre for Environmental Prediction meteorology (http://www.ncep.noaa.gov/) and Oregon Tidal Prediction Software (http://volkov.oce.orst.edu/tides/otps.html) using bathymetry derived from the ETOP01 Earth topography model (https://www.ngdc.noaa.gov/mgg/global). The resulting PCs were correlated against the respective $\delta^{18}O_{PC1\text{-}S1\text{-}3}$ series and the significance of the correlations tested (Figure 3). Bottom water salinity was not included in this analysis.

Finally, given the shallow depth and habitat restriction to continental shelf seas of the long-lived marine bivalves used in our reconstructions, we examine the potential influence of including only a limited number of $\delta^{18}O_{shell}$ series from such regions in our spatial network. We constructed a purely "hypothetical" spatial network using SST data derived from up to 25 independent 5° × 5° grid boxes in the HadISST1 data set from across the North Atlantic region (Figure S9). Sites included in the hypothetical proxy network were (1) constrained to the continental margins (14 sites), to simulate the inclusion of additional sclerochronological records that can only be constructed in shelf sea locations, and (2) across the entire North Atlantic Ocean (25 sites; Figure S9), to simulate a multiproxy approach that could include the addition of high-resolution sediment core records. The resulting hypothetical composites were then correlated against mean North Atlantic SSTs over the 20th century to evaluate whether increasing the spatial coverage (and number) of records significantly improved the skill of the resulting network. Only SST data were used for these analyses due to a lack of salinity mixing line equations from across the entire study area. As no proxy is a perfect record of SST, clearly using instrumental data to simulate these theoretical reconstructions will likely lead to an overestimate of the absolute skill of the resulting composite series. However, these analyses do provide an indication of whether increasing the number of proxy series would result in an overall increase in skill of the resulting network.

### 2.4. Environmental Analyses and Reconstruction Skill

To evaluate the sensitivity of the proxy and instrumental based composite series to North Atlantic marine variability, the $\delta^{18}O_{PC1\text{-}S1\text{-}3}$, $\delta^{18}O_{PC2\text{-}S1\text{-}2}$, $SST_{PC1}$, $SSS_{PC1}$, and $\delta^{18}O_{syn\_PC1}$ series were correlated against gridded SST (HadISST1; Rayner et al., 2003) and SSS (EN4 SSS; Good et al., 2013) data sets over the North Atlantic region using point correlation analyses. The point correlations were conducted using both raw (undetrended) and linear detrended annually averaged data over the 20th century using the KNMI Climate Explorer (Figure 4; Trouet & van Oldenborgh, 2013). To provide a quantitative assessment of the identified spatial sensitivities, monthly SST and SSS data were obtained from the HadISST1 and EN4 SSS data sets for the tropical North Atlantic (0–40°N by 0–80°W), subpolar gyre (SPG; 50–60°N by 20–60°W) regions, and between northern Scotland and the Faroe Isles (57–67°N by 0–10°W) to broadly reflect the northern trajectory of the North Atlantic Current (NAC). Linear regression analyses were then performed between the composite series and the mean monthly, annual mean, and seasonal mean SSTs and SSSs over the three regions (tropical North Atlantic, SPG, and NAC; Figures 5 and S7).

A split calibration and verification statistical approach was used to calibrate the $\delta^{18}O_{PC1\text{-}S1\text{-}3}$ and $\delta^{18}O_{PC2\text{-}S1\text{-}2}$ series against the target SST and SSS time series and to evaluate the level of skill the calibrated time series has in reconstructing the target parameter (North et al., 2000). The

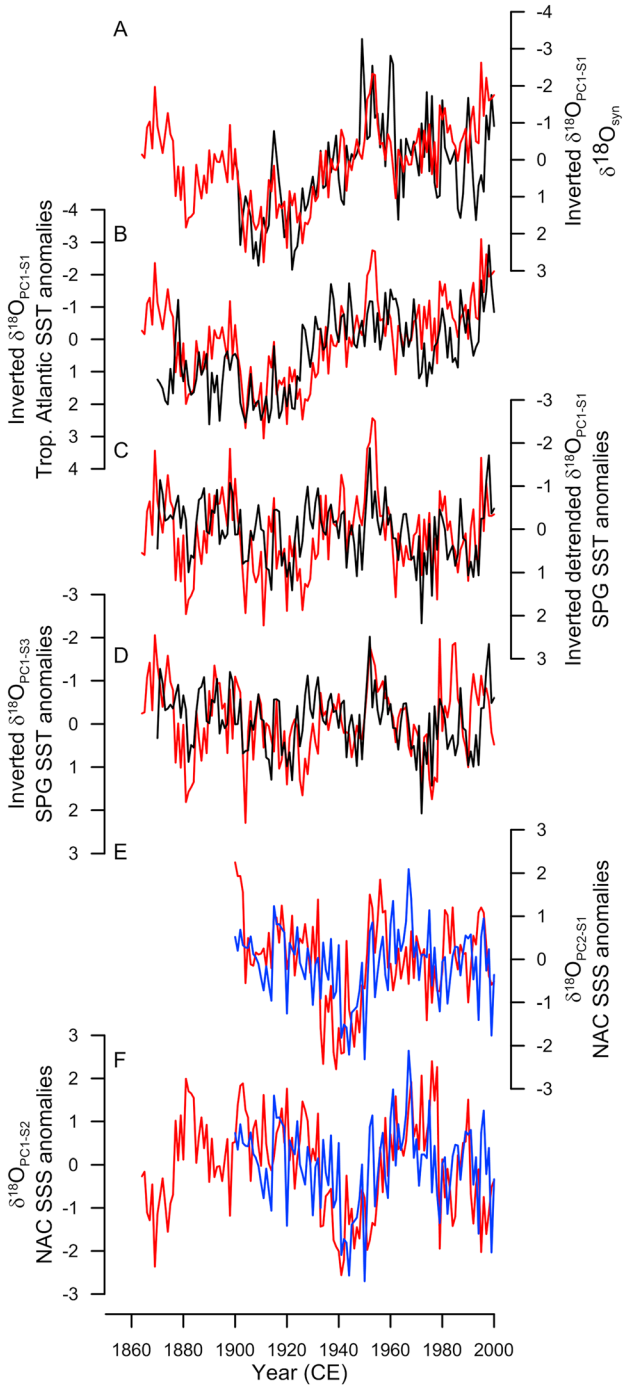


**Figure 5.** Comparison of the temporal and spatial sensitivity of the $\delta^{18}O_{PC1-S1-S3}$ and $\delta^{18}O_{PC2-S1}$ series against North Atlantic sea surface temperatures (SSTs) and sea surface salinity (SSS). (a) The inverted $\delta^{18}O_{PC1-S1}$ (red line) and $\delta^{18}O_{syn-PC1}$ (black line) series. (b) Tropical North Atlantic SST anomalies (black) plotted with the $\delta^{18}O_{PC1-S1}$ series (red line); (c and d) SST anomalies from the subpolar gyre (black lines) plotted with the inverted (c) detrended $\delta^{18}O_{PC1-S1}$ and (d) the $\delta^{18}O_{PC1-S3}$ series respectively (red lines). SSS anomalies from the North Atlantic Current (blue lines) plotted with (e) the $\delta^{18}O_{PC2-S1}$ and (f) the $\delta^{18}O_{PC1-S2}$ series. The instrumental data plotted in (b–f) are calculated as the mean SST/SSS of the data derived from the HadISST1 and EN4 SSS data sets over the areas highlighted by the black box inserts in Figures 4b–4d and 4k and 4l, respectively.

calibration was generated using linear regression analyses between the $\delta^{18}O_{PC1-S1-3}$ and $\delta^{18}O_{PC2-S1-2}$ series and the target parameters, tropical North Atlantic SSTs [HadISST1], SPG SSTs [HadISST1], and NAC SSSs [EN4 SSS], over the period containing the strongest correlation (either 1900–1949 or 1950–2000, respectively). The portion of the gridded data not used for the calibration therefore remained independent and was used to verify and estimate the skill of the final reconstruction. The calibration was then applied to convert the full length $\delta^{18}O_{PC1-S1-3}$ and $\delta^{18}O_{PC2-S1-2}$ series to SSTs and SSSs. While gridded data products spanning the early half of the 20th century contain increased uncertainty, these data still provide a useful indication of the ability of the calibrated reconstruction to track the long-term changes in SST and SSS variability over this region. Mean square errors were calculated between the calibrated $\delta^{18}O_{PC1-S1-3}$ series and the target parameters over both the calibration and verification periods, and reduction of error (RE) and coefficient of efficiency (CE) statistics calculated using the Ebisuzaki Monte Carlo methodology (Macias-Fauria et al., 2012). The calibration and verification statistics were estimated using the ReconStats package in Matlab R2015a (Macias-Fauria et al., 2012).

Multiple linear regression analyses were used to examine the total percentage variance that the SPG and tropical North Atlantic SST explain in the $\delta^{18}O_{PC1-S1}$ series. These analyses were conducted using R V3.4.1.

### 2.5. Assessing the Sensitivity to North Atlantic Circulation Dynamics

As the $\delta^{18}O_{PC1-S1-3}$ and $\delta^{18}O_{PC2-S1}$ series do not overlap with the RAPID observational record of North Atlantic transport at 26.5°N (Smeed et al., 2016), and only by a few years with the SPG index (Hatun et al., 2005), it is not possible to directly evaluate the covariance between direct measurements of North Atlantic circulation dynamics and the $\delta^{18}O_{PC1-S1-3}$/$\delta^{18}O_{PC2-S1}$ series. We therefore analyzed the $\delta^{18}O_{PC1-S1-3}$ and $\delta^{18}O_{PC2-S1}$ series against a tide-gauge based reconstruction of European Slope Current (ESC) strength (ESC annual index, Marsh et al., 2017). The strength of the ESC is associated with both Ekman transport and seawater density gradients (Huthnance, 1984) and is positively linked with both changes in SPG and Atlantic Meridional Overturning Circulation strength (Marsh et al., 2017). The $\delta^{18}O_{PC1-S1-3}$ and $\delta^{18}O_{PC2-S1}$ series were correlated against the ESC annual index using linear regression analyses over the interval from 1957 to 2000. These analyses were conducted using linear detrended data to remove the influence of long-term atmospheric warming not associated with changes in ESC strength.

To evaluate the influence of atmospheric circulation patterns on driving the variability in the proxy composite series, the proxy composite series were correlated against gridded sea level pressure (SLP; Trenberth & Paolino, 1980) and zonal wind stress data sets (20th century reanalysis V2 data acquired from the NOAA/OAR/ESRL PSD available at www.esrl.noaa.gov/psd/) over the 20th century. The correlations were calculated using KNMI Climate Explorer (Figure S10).

## 3. Results and Discussion

### 3.1. Spatial Network Construction

Despite the large distances between each of the sampling locations significant, albeit weak, Pearson correlations were identified between

the four independent $\delta^{18}O_{shell}$ series (e.g., $R = 0.30$ $P < 0.1$; $R = 0.37$ $P < 0.05$ calculated between the Scottish and Gulf of Maine series and between the Iceland and the Gulf of Maine $\delta^{18}O_{shell}$ series; Figure S1 and Table S2). Despite the relatively weak correlations identified between the four independent $\delta^{18}O_{shell}$ series, the nested PCA resulted in the generation of significant (eigenvalues $> 1$) primary PCs using all three PCA strategies for the full period of 1864–2000 and the generation of significant secondary PCs using strategies 1 and 2 (Figure 2). The $\delta^{18}O_{PC2\text{-}S1\text{-}2}$ series were only significant over the period represented by all four individual $\delta^{18}O_{shell}$ series (1900–2000). Comparison of the replicated proxy composite series generated using PCA of different combinations of three out of the four independent $\delta^{18}O_{shell}$ series identified significant correlations between the resulting PCs ($R = 0.74$–$0.97$; Table S3 and Figure S3) and consistently high eigenvalues (1.41–1.73) and percentage variance statistics (43.6–55.1%). This result implies that there is no strong bias in the resulting composite series toward any of the four independent $\delta^{18}O_{shell}$ series. The identification of coherence between the four independent $\delta^{18}O_{shell}$ series, and generation of significant PCs (i.e., composite series), despite the large distances between the four locations, suggests that a suite of common environmental mechanisms are likely driving variability across the four sampling localities (Cunningham et al., 2013; Wilson et al., 2016). Such a result is perhaps not surprising given the previously identified connectivity of the hydrographic settings of the four sampling locations to wider North Atlantic Ocean variability (Mette et al., 2016; Reynolds et al., 2016; Reynolds, Hall, et al., 2017; Wanamaker et al., 2008, 2011).

The application of the PCA, using all three strategies, on the instrumental SST, SSS, $\delta^{18}O_{syn}$ data, and model-derived bottom water temperature data generated PCs with significant eigenvalues ($>1$). However, while the PCA of the $\delta^{18}O_{syn}$ data generated a robust PC1, using strategy 1, the eigenvalues for PC2 were $<1$ and therefore the $\delta^{18}O_{syn\text{-}PC2}$ data were not utilized in any further analyses. Linear regression analyses identified significant coherence between the $\delta^{18}O_{PC1\text{-}S1}$ series and the composites generated using instrumental SST and $\delta^{18}O_{syn}$ ($SST_{PC1}$ $R = -0.50$, $P < 0.05$ and $\delta^{18}O_{syn\text{-}PC1}$ $R = 0.55$, $P < 0.05$; calculated over the 20th century; Figure S6). No significant correlation was identified between the $\delta^{18}O_{PC1\text{-}S1}$ series and the composite derived using SSS across the four sampling locations ($SSS_{PC1}$ $R = -0.37$ $P = 0.18$; Figure S6). These results suggest that SST variability at the sampling locations dominates the variability in the $\delta^{18}O_{PC1\text{-}S1}$ series. However, taking both SST and SSS variability into account (using the $\delta^{18}O_{syn\text{-}PC1}$ record) leads to a marginal improvement of the sensitivity of the proxy composite series to environmental variability.

The comparison of the proxy derived composites ($\delta^{18}O_{PC1\text{-}S1\text{-}3}$) against the $\delta^{18}O_{syn}$ and model-derived composites highlights that the proxy composite series are, with the exception of the $\delta^{18}O_{PC1\text{-}S3}$ and $\delta^{18}O_{syn\text{-}S3}$ series, significantly coherent ($P < 0.1$) with the variability contained in the instrumental and model based composite series (Figure 3). While the $\delta^{18}O_{PC1\text{-}S3}$ and $\delta^{18}O_{syn\text{-}S3}$ series exhibit no significant coherence, the $\delta^{18}O_{PC1\text{-}S3}$ series and corresponding model derived composite series do significantly correlate ($R = 0.40$ $P < 0.05$; Figure 3). Given that the eigenvalue and percentage variance statistics for these series are significant, it is unlikely that the resulting composite series contain significant nonenvironmentally driven variability. We therefore suggest that the lack of coherence between the $\delta^{18}O_{PC1\text{-}S3}$ and $\delta^{18}O_{syn\text{-}S3}$ series stems from differences in temperature and salinity variability between sea surface and bottom water conditions at the sampling sites. While the gridded data products used to generate the pseudo proxy network are a measure of surface water conditions, the shells used to generate the proxy network were collected at a range of water depths between 6 and 80 m. Comparison of the proxy-derived composite $\delta^{18}O_{PC1\text{-}S1\text{-}3}$ series with composites derived utilizing modeled bottom water temperature data support this hypothesis, with significant coherence found between the proxy and model-derived composites generated using all three strategies (Figure 3). These results strongly support the conclusions of recent marine proxy and pseudo-proxy based studies in the Northeast Atlantic (Pyrina et al., 2017; Reynolds, Richardson, et al., 2017) and the North Pacific (Black, 2009; Black et al., 2014) that multiple sclerochronological records can be used as part of a spatial network approach to investigate past marine variability.

Variability contained in the $\delta^{18}O_{PC1\text{-}S1}$ series is dominated by a gradual increase in $\delta^{18}O$ over the period from 1864 to ca. 1900 and a significant linear decrease in $\delta^{18}O$ over the 20th century ($R = -0.74$, $P < 0.001$). The $\delta^{18}O_{PC1\text{-}S2\text{-}3}$ and $\delta^{18}O_{PC2\text{-}S1\text{-}2}$ series are dominated by multidecadal scale variability and contain no significant long-term trends. In the case of the $\delta^{18}O_{PC1\text{-}S2\text{-}3}$ series, such a result is to be expected as the PCA strategies employed broadly act as 50- and 30-year high pass filters, respectively.

**Table 1**
*Calibration and Verification Statistics Calculated Between the $\delta^{18}O_{PC1\text{-}S1\text{-}3}$ and $\delta^{18}O_{PC2\text{-}S1}$ Series and North Atlantic SSTs and SSS*

| Proxy | Target parameter | $R$ | $R^2$ | RE | CE |
|---|---|---|---|---|---|
| $\delta^{18}O_{PC1\text{-}S1}$ | Annual Tropical Atlantic SSTs | −0.64 | 0.41 | 0.52 | 0.14 |
| $\delta^{18}O_{PC1\text{-}S1}$ detrended | Summer SPG SSTs | −0.39 | 0.15 | 0.08 | 0.08 |
| $\delta^{18}O_{PC1\text{-}S3}$ | Summer SPG SSTs | −0.34 | 0.12 | 0.12 | 0.12 |
| $\delta^{18}O_{PC1\text{-}S2}$ | Summer SPG SSTs | −0.31 | 0.10 | 0.08 | 0.07 |
| $\delta^{18}O_{PC2\text{-}S1}$ | Winter NAC SSS | 0.42 | 0.18 | 0.12 | 0.11 |
| $\delta^{18}O_{PC1\text{-}S2}$ | Winter NAC SSS | 0.40 | 0.16 | 0.18 | 0.17 |

*Note*. The correlation statistics are calculated over the entire 20th century. The correlation confidents, reduction of error (RE), and coefficient of efficiency (CE) statistics are calculated using Ebisuzaki Monte Carlo methodology using 1,000 reanalyzes. The RE and CE statistics are significant if ≥0. All correlations shown in the table are significant at a level of $P < 0.05$.

### 3.2. Environmental Analyses and Reconstruction Skill

A range of significant relationships were identified using point correlation analyses between the proxy-based composites and gridded SST (HadISST1) and SSS (EN4 SSS) data sets across the North Atlantic region over the 20th century (Figure 4). In particular, the $\delta^{18}O_{PC1\text{-}S1}$ series contains significant coherence ($P < 0.1$) with mean annual SSTs across the tropical North Atlantic from 0 to 40°N across the entire width of the North Atlantic basin and between variability contained in the $\delta^{18}O_{PC1\text{-}F}$ series, $\delta^{18}O_{PC1\text{-}S2\text{-}3}$, and $\delta^{18}O_{PC2\text{-}S1}$ series and variability in mean summer SSTs across regions of the North Atlantic broadly corresponding with the SPG (Figure 4). Quantitative examination of the point correlations, using linear regression analysis, shows peak correlation between the $\delta^{18}O_{\text{-}PC1\text{-}S1}$ series and mean annual tropical Atlantic SSTs ($R = -0.64$ $P < 0.05$; Figure 5) and between the $\delta^{18}O_{PC1\text{-}F}$, $\delta^{18}O_{PC1\text{-}S2\text{-}3}$, and $\delta^{18}O_{PC2\text{-}S1}$ series and mean summer SPG SSTs ($R = -0.31$, $-0.34$, and $-0.39$ respectively, $P < 0.05$; Figures 4 and 5). The point correlations identified between the proxy based composite series and HadISST1 data are consistent with the relationship observed between the $\delta^{18}O_{syn}$-based composites and the HadISST data (Figure 4a). The strong coherence between the spatial distribution, and sign, of the point correlations calculated between the $\delta^{18}O_{PC1\text{-}S1}$ and $\delta^{18}O_{syn\text{-}PC1}$ series when correlated against gridded SST and SSS products (Figure 4) demonstrates that the variability extracted by the nested PCA, and its sensitivity to basin-scale ocean dynamics, is reproducible and, over the observational instrumental period, predictable using independent instrumental-based records.

Examination of the point correlations generated between the $\delta^{18}O_{PC1\text{-}S1\text{-}3}$ and $\delta^{18}O_{PC1\text{-}F}$ (generated by high pass filtering the individual $\delta^{18}O_{shell}$ series; Figures 4 and S8) suggests differences in the spatial sensitivity of the proxy-based composites depending upon the time scale of variability contained in the composite series. For example, variability contained in the $\delta^{18}O_{PC1\text{-}S1}$ series, which incorporates both high and low frequency variability, contains a strong coherence with variability in the tropical North Atlantic. However, the $\delta^{18}O_{PC1\text{-}S2\text{-}3}$ and $\delta^{18}O_{PC1\text{-}F}$, which contain only subcentennial scale variability, exhibit the strongest correlations with SST variability over the SPG region of the North Atlantic (Figure S8). Given that both the $\delta^{18}O_{PC1\text{-}S2\text{–}3}$ and $\delta^{18}O_{PC1\text{-}F}$ series exhibit similar sensitivity to SPG, SSTs suggest that the coherence is associated with the time scale of variability contained in the records and not associated with the methodologies used to generate the composite series. These analyses also highlight significant correlations with between the $\delta^{18}O_{PC1\text{-}F}$ composites and tropical Atlantic SSTs; however, the correlations are weaker in nature than those identified in the analysis using the $\delta^{18}O_{PC1\text{-}S1}$ series. These analyses therefore suggest that the coherence between the $\delta^{18}O_{PC1\text{-}S1}$ and tropical North Atlantic SSTs is likely associated with longer time scale (centennial) variability, while the high frequency (subcentennial) variability in the proxy composites is associated with SPG variability. This interpretation is supported by the examination of multiple linear regression analyses that highlights that SPG and tropical Atlantic SST variability can explain 41% ($P < 0.001$) of the variability in the $\delta^{18}O_{PC1\text{-}S1}$ series. However, multiple linear regression analyses indicate that subcentennial SPG and centennial tropical Atlantic SST variability can explain 61% of the variability in the $\delta^{18}O_{PC1\text{-}S1}$ series.

In addition to the strong coherence with SST variability, the point correlation analyses also identified significant coherence between the proxy-based composite series and SSS variability (EN4 SSS) over the Norwegian Sea and along the coast of Nova Scotia respectively (Figure 4). The point correlations identified significant correlations ($P < 0.1$) between the $\delta^{18}O_{PC1\text{-}S2}$ and $\delta^{18}O_{PC2\text{-}S1}$ series when correlated against mean winter SSS variability over the region of the North Atlantic between the northern British Isles and Iceland and across the Norwegian Sea (Figures 4k and 4l). Linear regression analyses between the $\delta^{18}O_{PC1\text{-}S2}$ and $\delta^{18}O_{PC2\text{-}S1}$ series and SSS data obtained from this region (57–67°N by 0–10°W) highlight the significant nature of the coherence between the $\delta^{18}O_{PC1\text{-}S2}$ and $\delta^{18}O_{PC2\text{-}S1}$ series and mean winter NAC SSS ($R = 0.40$ and 0.42, respectively, $P < 0.05$; Figures 4 and 5).

The correlations between the hypothetical proxy network, constructed using different numbers of theoretical proxy records (based on observational SST data) from the continental margins and across the North

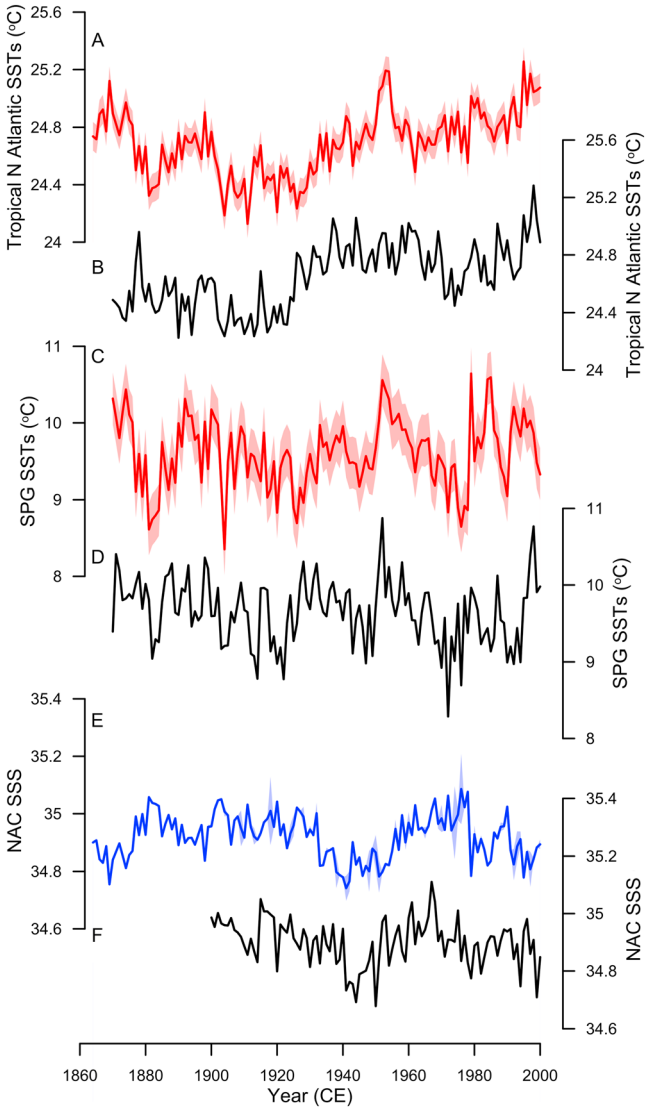


**Figure 6.** (a and b) Reconstructed (red line) and observed (black line) tropical North Atlantic sea surface temperatures (SSTs), respectively. (c and d) Reconstructed (red line) and observed subpolar gyre SSTs, respectively. (e and f) Reconstructed (blue line) and observed (black line) winter sea surface salinity in the North Atlantic Current. The shaded red and blue areas around a, c, and e represent the 2 times mean square error uncertainty envelope.

Atlantic Ocean, against mean North Atlantic SSTs indicate that increasing the number of proxy records would increase the sensitivity of the resulting composite series to wider North Atlantic SSTs. The correlation increases from $R = 0.68$ ($P < 0.001$), when using the $SST_{PC1}$ series generated using the four sampling location used in this study, up to $R = 0.81$ ($P < 0.001$) when using 14 shelf sea sampling locations. The correlation increases further to $R = 0.93$ ($P < 0.001$) if these 14 shelf sea records could be integrated with records from the central North Atlantic region. As no proxy record has absolute skill at reconstructing local SSTs, these values are an overestimate of the likely ability of the proxy-based network to reconstruct North Atlantic North Atlantic SSTs. However, while the precise degree of coherence may vary, these analyses do demonstrate that increasing the number of independent shelf sea sclerochronological records included in our network would be beneficial and enhance our ability to skillfully reconstruct open ocean variability. At present there are no annually resolved surface ocean proxy records available from the central North Atlantic Ocean that could be included in the network, but there are numerous high-resolution sediment core proxy records that could potentially be utilized. While integrating mixed archive proxy records with variable age and proxy uncertainties would inherently add complexity to the construction of a spatial network (Cunningham et al., 2013; McGregor et al., 2015), our hypothetical considerations suggest that integrating records from this region would potentially increase the ability of the network to reconstruct past central North Atlantic Ocean variability, especially at decadal to multidecadal time scales.

The split calibration-verification methodology quantitatively evaluated the skill of each of the proxy composite series at reconstructing the selected target parameter. The resulting RE and CE statistics were positive for each of the proxy-based reconstructions of the respective target parameters (Table 1). The RE and CE statistics are significant if greater than zero, indicating that the corresponding reconstructions contain significant skill at reconstructing the target parameters. These results indicate that the calibrated $\delta^{18}O_{PC1\text{-}S1}$ series provides a skillful reconstruction of tropical North Atlantic SSTs, the $\delta^{18}O_{PC1\text{-}S2}$ series skillful reconstructions of NAC SSTs and SPG SSTs, the $\delta^{18}O_{PC1\text{-}S2}$ series skillful reconstructions of mean summer SPG SSTs, and the $\delta^{18}O_{PC2\text{-}S1}$ series a skillful reconstruction of winter NAC SSTs (Figure 6).

### 3.3. Sensitivity to Ocean and Atmospheric Circulation

The identification of significant correlations between the $\delta^{18}O_{PC1\text{-}S1\text{-}3}$ series and tropical North Atlantic SSTs, SPG SSTs, and NAC SSSs highlights the significance of the interplay between the tropical and subpolar North Atlantic dynamics in modulating environmental variability across the continental shelf seas of the North Atlantic Ocean. Given the time it takes for signals to propagate northward through the surface ocean from the equatorial Atlantic to the subpolar latitudes (Getzlaff et al., 2005), these results suggest that both marine and atmospheric circulation patterns are playing a role in driving the common variability across the four independent $\delta^{18}O_{shell}$ series.

The linear regression analyses between the linear detrended $\delta^{18}O_{PC1\text{-}S1\text{-}S3}$ series and the ESC annual index (Marsh et al., 2017) identified a range of correlations ($\delta^{18}O_{PC1\text{-}S1}$ $R = -0.14$, $P > 0.1$; $\delta^{18}O_{PC1\text{-}S2}$ $R = -0.30$, $P = 0.06$; $\delta^{18}O_{PC1\text{-}S3}$ $R > -0.1$ $P > 0.1$). Examination of the correlations between the linear detrended 5-year first-order loess low-pass filtered linear detrended series demonstrates a marked increase in the strength of the correlations ($\delta^{18}O_{PC1\text{-}S1}$ $R = -0.27$, $P > 0.1$; $\delta^{18}O_{PC1\text{-}S2}$ $R = -0.62$, $P < 0.01$; $\delta^{18}O_{PC1\text{-}S3}$ $R = -0.57$ $P < 0.05$). The identification of significant correlations between the $\delta^{18}O_{PC1\text{-}S3}$ series and the ESC annual

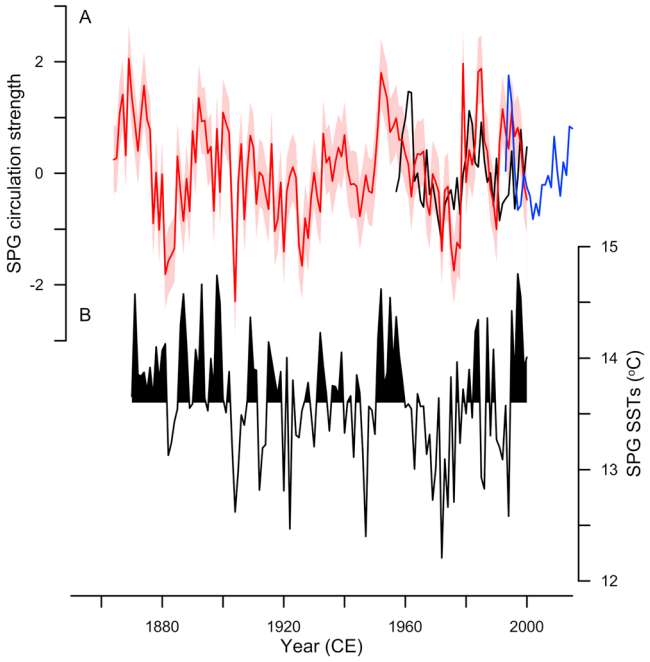


**Figure 7.** (a) Comparison between the $\delta^{18}O_{PC1\text{-}S3}$ series (red line and shaded red envelope) and the Marsh et al. (2017) European Slope Current annual index (black line) and the Hatun et al. (2005) subpolar gyre (SPG) index (blue line). (b) Mean annual SPG HadISST1 sea surface temperatures (SSTs; black line) with years containing SSTs greater than the mean shaded in black.

index, most notably using the 5-year smoothed linear detrended data ($\delta^{18}O_{PC1\text{-}S2}$ and $\delta^{18}O_{PC1\text{-}S3}$), strongly suggests that the variability captured by the proxy composite series is, in part, associated with the advection of warm and salty waters through the North Atlantic Ocean surface circulation. These analyses indicate that periods of enhanced (reduced) ESC strength (by extension SPG strength, Hatun et al., 2005) coincide with periods of warm (cold) SPG SSTs and lower (higher) $\delta^{18}O_{PC1\text{-}S2\text{-}3}$ values (Figure 7). The relatively weak coherence with interannual variability, however, suggests that other mechanisms mask the variability on inter-annual time scales.

The point correlation analyses between the proxy composite series against gridded SLP and zonal wind stress data yielded a range of significant correlations ($P < 0.1$; Figure S10). A dipole pattern of positive and negative correlations was identified over the tropical and polar North Atlantic regions respectively between the proxy composite series and SLPs using both linear detrended and nondetrended data sets (Figure S10). Similarly, a dipole pattern of correlations over the tropical and subpolar regions of the North Atlantic was identified in the correlations between the composite proxy series and zonal wind stress, also using both linear detrended and nondetrended data (Figure S10). The identification of significant correlations between the proxy series and both gridded SLP and zonal wind stress data sets strongly indicates that atmospheric circulation patterns play a role in propagating the tropical Atlantic and SPG temperature signals toward the coastal regions of the North Atlantic. These analyses are therefore in agreement with the proposed mechanisms and forcings identified by previous modeling efforts (e.g., Marsh et al., 2015). The sign, spatial distribution, and seasonality of the correlations between the proxy series and SLPs are characteristic of the dipole pressure gradient associated with the wNAO, with significant positive and negative correlations occurring during winter over the tropical and polar regions of the North Atlantic, respectively (Figure S10).

## 4. Conclusion

Although there are presently only a few individual $\delta^{18}O_{shell}$ records that span multicentennial to millennial time spans, these analyses highlight that applying nested PCA to a suite of sclerochronological $\delta^{18}O_{shell}$ records, from across the North Atlantic Ocean region, can facilitate the quantitative reconstruction of basin scale ocean dynamics. Supplementing the current network of $\delta^{18}O_{shell}$ records with additional sclerochronological and well-dated high-resolution sediment core proxy records of surface ocean variability will further enhance our ability to quantitatively investigate past ocean dynamics. While the application of terrestrial proxy-derived marine reconstructions (e.g., Gray, 2004; Mann et al., 2014; Rahmstorf et al., 2015) may currently provide significantly longer reconstructions, they lack independence from reconstructions of atmospheric dynamics (being based on the same tree ring series). This lack of independence between the marine and atmospheric reconstructions restricts our ability to analyze and quantify the influence that marine variability has on atmospheric climate variability. The development of independent marine reconstructions is therefore essential for the robust assessment of the past influence of marine variability on the climate system. The continued development of quantitative reconstructions of past marine variability will have a profound influence on our ability to validate numerical climate models and to help constrain uncertainties in near-term decadal scale climate predictions.

**Acknowledgments**
This work was supported in part by the Natural Environment Research Council funded Climate of the Last Millennium Project (project NE/N001176/1) and the National Science Foundation (grant 1417766 to ADW). The authors would like to thank the two anonymous reviewers for their constructive reviews that significantly improved this manuscript. The four $\delta^{18}O_{shell}$ records analyzed in this study are publicly available at https://www.ncdc.noaa.gov/data-access/paleoclimatology-data/datasets. The instrumental data used in this study are available at http://climexp.knmi.nl/.

## References

Black, B. A., Griffin, D., Van Der Sleen, P., Wanamaker, A. D., Speer, J. H., Frank, D. C., et al. (2016). The value of crossdating to retain high-frequency variability, climate signals, and extreme events in environmental proxies. *Global Change Biology*, *22*, 2582–2595.

Black, B. A. (2009). Climate-driven synchrony across tree, bivalve, and rockfish growth-increment chronologies of the northeast pacific. *Marine Ecology Progress Series*, *378*, 37–46. https://doi.org/10.3354/meps07854

Black, B. A., Sydeman, W. J., Frank, D. C., Griffin, D., Stahle, D. W., Garcia-Reyes, M., et al. (2014). Climate change. Six centuries of variability and extremes in a coupled marine-terrestrial ecosystem. *Science*, *345*, 1498–1502.

Cage, A. G., & Austin, W. E. N. (2010). Marine climate variability during the last millennium: The loch sunart record, Scotland, UK. *Quaternary Science Reviews*, *29*(13-14), 1633–1647. https://doi.org/10.1016/j.quascirev.2010.01.014

Cunningham, L. K., Austin, W. E., Knudsen, K. L., Eiriksson, J., Scourse, J. D., Wanamaker, A. D., et al. (2013). Reconstructions of surface ocean conditions from the Northeast Atlantic and nordic seas during the last millennium. *The Holocene*, *23*(7), 921–935. https://doi.org/10.1177/0959683613479677

Ebisuzaki, W. (1997). A method to estimate the statistical significance of a correlation when the data are serially correlated. *Journal of Climate*, *10*(9), 2147–2153. https://doi.org/10.1175/1520-0442(1997)010<2147:AMTETS>2.0.CO;2

Freeman, E., Woodruff, S. D., Worley, S. J., Lubker, S. J., Kent, E. C., Angel, W. E., et al. (2017). Icoads release 3.0: A major update to the historical marine climate record. *International Journal of Climatology*, *37*(5), 2211–2232. https://doi.org/10.1002/joc.4775

Getzlaff, J., Boning, C. W., Eden, C., & Biastoch, A. (2005). Signal propagation related to the North Atlantic overturning. *Geophysical Research Letters*, *32*, L09602. https://doi.org/10.1029/2004GL021002

Good, S. A., Martin, M. J., & Rayner, N. A. (2013). En4: Quality controlled ocean temperature and salinity profiles and monthly objective analyses with uncertainty estimates. *Journal of Geophysical Research: Oceans*, *118*, 6704–6716. https://doi.org/10.1002/2013JC009067

Gray, S. T. (2004). A tree-ring based reconstruction of the Atlantic multidecadal oscillation since 1567 A.D. *Geophysical Research Letters*, *31*, L12205. https://doi.org/10.1029/2004GL019932

Grossman, E., & Ku, T. (1986). Oxygen and carbon isotope fractionation in biogenic aragonite: Temperature effects. *Chemical Geology*, *59*, 59–74. https://doi.org/10.1016/0168-9622(86)90057-6

Hatun, H., Sando, A. B., Drange, H., Hansen, B., & Valdimarsson, H. (2005). Influence of the Atlantic subpolar gyre on the thermohaline circulation. *Science*, *309*(5742), 1841–1844. https://doi.org/10.1126/science.1114777

Huthnance, J. M. (1984). Slope currents and jebar. *Journal of Physical Oceanography*, *14*(4), 795–810. https://doi.org/10.1175/1520-0485(1984)014<0795:SCA>2.0.CO;2

Kennedy, J. J., Rayner, N. A., Smith, R. O., Parker, D. E., & Saunby, M. (2011). Reassessing biases and other uncertainties in sea surface temperature observations measured in situ since 1850: 2. Biases and homogenization. *Journal of Geophysical Research*, *116*, D14104. https://doi.org/10.1029/2010JD015220

Macias-Fauria, M., Grinsted, A., Helama, S., & Holopainen, J. (2012). Persistence matters: Estimation of the statistical significance of paleoclimatic reconstruction statistics from autocorrelated time series. *Dendrochronologia*, *30*(2), 179–187. https://doi.org/10.1016/j.dendro.2011.08.003

Mann, M. E., Steinman, B. A., & Miller, S. K. (2014). On forced temperature changes, internal variability, and the amo. *Geophysical Research Letters*, *41*, 3211–3219. https://doi.org/10.1002/2014GL059233

Mann, M. E., Zhang, Z., Rutherford, S., Bradley, R. S., Hughes, M. K., Shindell, D., et al. (2009). Global signatures and dynamical origins of the little ice age and medieval climate anomaly. *Science*, *326*(5957), 1256–1260. https://doi.org/10.1126/science.1177303

Marsh, R., Haigh, I. D., Cunningham, S. A., Inall, M. E., Porter, M., & Moat, B. I. (2017). Large-scale forcing of the European Slope Current and associated inflows to the north sea. *Ocean Science*, 13.

Marsh, R., Hickman, A. E., & Sharples, J. (2015). S2p3-r (v1.0): A framework for efficient regional modelling of physical and biological structures and processes in shelf seas. *Geoscientific Model Development*, *8*(10), 3163–3178. https://doi.org/10.5194/gmd-8-3163-2015

Marzocchi, A., Hirschi, J. J. M., Holliday, N. P., Cunningham, S. A., Blaker, A. T., & Coward, A. C. (2015). The North Atlantic subpolar circulation in an eddy-resolving global ocean model. *Journal of Marine Systems*, *142*, 126–143. https://doi.org/10.1016/j.jmarsys.2014.10.007

McGregor, H. V., Evans, M. N., Goosse, H., Leduc, G., Martrat, B., Addison, J. A., et al. (2015). Robust global ocean cooling trend for the pre-industrial common era. *Nature Geoscience*, *8*, 671.

Mette, M. J., Wanamaker, A. D. Jr., Carroll, M. L., Ambrose, W. G. Jr., & Retelle, M. J. (2016). Linking large-scale climate variability with arctica islandica shell growth and geochemistry in northern Norway. *Limnology and Oceanography*, *61*(2), 748–764. https://doi.org/10.1002/lno.10252

Moberg, A., Sonechkin, D. M., Holmgren, K., Datsenko, N. M., & Karlen, W. (2005). Highly variable northern hemisphere temperatures reconstructed from low- and high-resolution proxy data. *Nature*, *433*(7026), 613–617. https://doi.org/10.1038/nature03265

North, G. R., Biondi, F., Bloomfield, P., Christy, J. R., Cuffey, K. M., Dickinson, R. E., et al. (2000). *Surface temperature reconstructions for the last 2,000 years*. New York: The National Academies Press.

Pyrina, M., Wagner, S., & Zorita, E. (2017). Pseudo-proxy evaluation of climate field reconstruction methods of North Atlantic climate based on an annually resolved marine proxy network. *Climate of the Past*, *13*(10), 1339–1354. https://doi.org/10.5194/cp-13-1339-2017

Rahmstorf, S., Box, J. E., Feulner, G., Mann, M. E., Robinson, A., Rutherford, S., & S. E. J. (2015). Exceptional twentieth-century slowdown in Atlantic Ocean overturning circulation. *Nature Climate Change*, *5*, 475–480.

Rayner, N. A., Parker, D. E., Horton, E. B., Folland, C. K., Alexander, L. V., Rowell, D. P., et al. (2003). Global analyses of sea surface temperature, sea ice, and night marine air temperature since the late nineteenth century. *Journal of Geophysical Research*, *108*(D14), 4407. https://doi.org/10.1029/2002JD002670

Reynolds, D. J., Hall, I. R., Slater, S., Scourse, J. D., Halloran, P. R., & Sayer, M. D. J. (2017). Reconstructing past seasonal to multi-centennial scale variability in the NE Atlantic Ocean using the long-lived marine bivalve Mollusc glycymeris glycymeris. *Paleocanography*, *32*, 1153–1173. https://doi.org/10.1002/2017PA003154

Reynolds, D. J., Richardson, C. A., Scourse, J. D., Butler, P. G., Hollyman, P., Roman-Gonzalez, A., & Hall, I. R. (2017). Reconstructing North Atlantic marine climate variability using an absolutely-dated sclerochronological network. *Palaeogeography Palaeoclimatology Palaeoecology*, *465*, 333–346. https://doi.org/10.1016/j.palaeo.2016.08.006

Reynolds, D. J., Scourse, J. D., Halloran, P. R., Nederbragt, A. J., Wanamaker, A. D., Butler, P. G., et al. (2016). Annually resolved north atlantic marine climate over the last millennium. *Nature Communications*, 7.

Smeed, D., Mccarthy, G., Rayner, D., Moat, B. I., Johns, W. E., Baringer, M. O. & Meinen, C. S. (2016). *Atlantic Meridional Overturning Circulation observed by the rapid-mocha-wbts (rapid-meridional overturning circulation and heatflux array-western boundary time series) array at 26n from 2004 to 2015*. Liverpool, UK: British Oceanographic Data Centre—Natural Environment Research Council, UK. Retrieved from https://www.bodc.ac.uk/data/published_data_library/catalogue/10.5285/1a774e53-7383-2e9a-e053-6c86abc0d8c7/

Smith, L. M., Andrews, J. T., Castañeda, I. S., Kristjánsdóttir, G. B., Jennings, A. E., & Sveinbjörnsdóttir, Á. E. (2005). Temperature reconstructions for sw and n Iceland waters over the last 10calka based on δ18o records from planktic and benthic foraminifera. *Quaternary Science Reviews*, *24*(14-15), 1723–1740. https://doi.org/10.1016/j.quascirev.2004.07.025

Smith, T. M., Reynolds, R. W., Peterson, T. C., & Lawrimore, J. (2008). Improvements to noaa's historical merged land-ocean surface temperature analysis (1880–2006). *Journal of Climate*, *21*(10), 2283–2296. https://doi.org/10.1175/2007JCLI2100.1

Trenberth, K. E., & Paolino, D. A. (1980). The northern hemisphere sea-level pressure data set—Trends, errors and discontinuities. *Monthly Weather Review*, *108*(7), 855–872. https://doi.org/10.1175/1520-0493(1980)108<0855:TNHSLP>2.0.CO;2

Trouet, V., & van Oldenborgh, G. J. (2013). Climate explorer: A web-based research tool for high-resolution paleoclimatology. *Tree-Ring Research*, *69*(1), 3–13. https://doi.org/10.3959/1536-1098-69.1.3

Wanamaker, A. D. Jr., Kreutz, K. J., Schoene, B. R., & Introne, D. S. (2011). Gulf of Maine shells reveal changes in seawater temperature seasonality during the medieval climate anomaly and the little ice age. *Palaeogeography Palaeoclimatology Palaeoecology*, *302*(1-2), 43–51. https://doi.org/10.1016/j.palaeo.2010.06.005

Wanamaker, A. D., Kreutz, K. J., Schoene, B. R., Pettigrew, N., Borns, H. W., Introne, D. S., et al. (2008). Coupled North Atlantic slope water forcing on gulf of Maine temperatures over the past millennium. *Climate Dynamics*, *31*(2-3), 183–194. https://doi.org/10.1007/s00382-007-0344-8

Whitney, N. M., Wanamaker, A. D., Kreutz, K. J., & Introne, D. S. (2017). Spatial and temporal variability in the delta o-18(w) and salinity compositions of gulf of Maine coastal surface waters. *Continental Shelf Research*, *137*, 163–171. https://doi.org/10.1016/j.csr.2017.02.006

Wilson, R., Anchukaitis, K., Briffa, K. R., Buentgen, U., Cook, E., D'arrigo, R., et al. (2016). Last millennium northern hemisphere summer temperatures from tree rings: Part I: The long term context. *Quaternary Science Reviews*, *134*, 1–18. https://doi.org/10.1016/j.quascirev.2015.12.005

Wilson, R., Cook, E., D'arrigo, R., Riedwyl, N., Evans, M. N., Tudhope, A., & Allan, R. (2010). Reconstructing enso: The influence of method, proxy data, climate forcing and teleconnections. *Journal of Quaternary Science*, *25*(1), 62–78. https://doi.org/10.1002/jqs.1297